IOP Publishing Journal of Physics D: Applied Physics

J. Phys. D: Appl. Phys. **47** (2014) 475203 (11pp) doi:10.1088/0022-3727/47/47/475203

Atmospheric pressure plasma jets interacting with liquid covered tissue: touching and not-touching the liquid

Seth A Norberg[1], Wei Tian[2], Eric Johnsen[1] and Mark J Kushner[3]

[1] Department of Mechanical Engineering, University of Michigan, 2350 Hayward Street, Ann Arbor, MI 48109-2125 USA
[2] Department of Nuclear Engineering and Radiological Science, University of Michigan, 2355 Bonisteel Boulevard, Ann Arbor, MI 48109-2104 USA
[3] Department of Electrical Engineering and Computer Science, University of Michigan, 1301 Beal Avenue, Ann Arbor, MI 48109-2122, USA

E-mail: norbergs@umich.edu, ejohnsen@umich.edu, bucktian@umich.edu and mjkush@umich.edu

Received 21 July 2014, revised 7 September 2014
Accepted for publication 26 September 2014
Published 5 November 2014

Abstract

In the use of atmospheric pressure plasma jets in biological applications, the plasma-produced charged and neutral species in the plume of the jet often interact with a thin layer of liquid covering the tissue being treated. The plasma-produced reactivity must then penetrate through the liquid layer to reach the tissue. In this computational investigation, a plasma jet created by a single discharge pulse at three different voltages was directed onto a 200 μm water layer covering tissue followed by a 10 s afterglow. The magnitude of the voltage and its pulse length determined if the ionization wave producing the plasma plume reached the surface of the liquid. When the ionization wave touches the surface, significantly more charged species were created in the water layer with $H_3O^+_{aq}$, $O_3^-{}_{aq}$, and $O_2^-{}_{aq}$ being the dominant terminal species. More aqueous OH_{aq}, H_2O_{2aq}, and O_{3aq} were also formed when the plasma plume touches the surface. The single pulse examined here corresponds to a low repetition rate plasma jet where reactive species would be blown out of the volume between pulses and there is not recirculation of flow or turbulence. For these conditions, N_xO_y species do not accumulate in the volume. As a result, aqueous nitrites, nitrates, and peroxynitrite, and the HNO_{3aq} and $HOONO_{aq}$, which trace their origin to solvated N_xO_y, have low densities.

Keywords: plasma jet, plasmas on liquids, atmospheric pressure plasma, plasma activated water

(Some figures may appear in colour only in the online journal)

1. Introduction

The use of atmospheric pressure plasma jets in the context of plasma medicine for wound healing, sterilization of surfaces and cancer treatment is an increasingly important area of research [1–3]. Often the surface being treated is cellular tissue, which is covered by a thin liquid layer of a blood serum-like liquid a few hundred microns thick [4]. Instead of directly interacting with the tissue, the plasma-produced neutral reactive species, ions and photons first react with the liquid layer. Gas phase species solvate into the liquid and undergo additional reactions before the plasma produced activation energy reaches the underlying tissue. Photolysis and photoionization from plasma-produced ultraviolet and vacuum-ultraviolet (UV/VUV) photons may directly produce active species (neutral reactive species and ions) in the top layer of the liquid that subsequently react to form other aqueous ions and neutral reactive species.

Many recent investigations have addressed the manner in which plasma jets produce reactivity in liquids, starting

with water [5–7]. The majority of these studies have used a rare-gas seeded with a small amount (usually <1%) of a reactive gas (e.g., O_2, N_2, H_2O) as the media flowing through the plasma tube, which is then exhausted into room air. RONS (reactive oxygen and nitrogen species) are directly produced in the plasma jet and by mixing with the ambient air [8]. Configurations using gas shrouds around the jet have been investigated to control the mixing of the ambient air with the jet to then control reactive species production [9, 10].

A parameter in these investigations is whether the plasma plume emanating from the jet contacts the liquid layer (touching) or is not in direct contact with the liquid layer (not-touching). Experimentally, this distinction is usually made on whether the luminous visible plume from the jet extends to the surface of the liquid. Significantly different results for the reactive species composition in the liquid have been reported based on whether the plasma jet is touching or not-touching the liquid [11]. The delivery of electric fields to the underlying tissue is also expected to be sensitive to the touching or not-touching conditions. In this paper, we discuss results from a computational investigation of plasma jets incident onto a thin water layer over a tissue-like dielectric. Different applied voltages are used which result in touching and not-touching configurations. The proportion and magnitude of aqueous charged and neutral species that diffuse to the underlying tissue depends on the touching or not-touching conditions. Aqueous ions diffusing through the liquid to the underlying tissue are significantly greater for touching conditions due to the rapid solvation of gas phase ions afforded by the contact. Neutral aqueous species produced by the jet are less sensitive to the touch or no-touch conditions, and scale more proportionately with the energy deposition per pulse in the jet.

The model used in this investigation is described in section 2. A comparison of touching and not-touching plasma jets onto thin liquid layers is discussed in section 3. Our concluding remarks are in section 4.

2. Description of model

The 2D cylindrically symmetric, plasma hydrodynamics model utilized in this investigation is *nonPDPSIM* which is executed on an unstructured mesh as described in detail in [12, 13]. For the purpose of this study, *nonPDPSIM* consists of three major modules—the plasma transport module, the radiation transport module and the fluid transport module. In the plasma transport module, Poisson's equation and continuity equations for all charged species (in the volume and on surfaces) are integrated in time using a fully implicit Newton-iteration technique [13]. Spatial derivatives and divergence operators are expressed in fully conservative finite-volume form. Each time step is then followed by an implicit update of the electron energy equation for electron temperature, neutral species continuity equations and radiation transport. Transport coefficients and rate coefficients for electrons as a function of electron temperature are obtained from solutions of the stationary Boltzmann's for the electron energy distribution. These tabulated coefficients which are interpolated during execution of the model are updated on sub-nanosecond time scales to reflect changing species and mole fractions. Radiation transport addresses photoionization of O_2 and H_2O in the gas phase, and photoionization and photo-dissociation of H_2O_{aq} in the liquid phase. (The subscript $_{aq}$ denotes aqueous or in liquid species.) This portion of the model is discussed in detail in [13, 14].

In the fluid module, a modified form of the Navier–Stokes equations (continuity, momentum, energy) are solved to produce the advective flow field while including body forces (e.g., momentum transfer from charged particles) and heat sources (e.g., Joule heating and change in enthalpy due to reactions) produced in the plasma transport module [15]. Since the gas constituents have large differences in atomic or molecular mass, the mass continuity equation is replaced by a number-density continuity equation and a fourth equation for the average molecular weight. These equations are simultaneously and implicitly solved using numerically derived Jacobian elements on the same unstructured mesh as the plasma calculation. The individual continuity equations for all species are simultaneously integrated using the advective flow field as a check for the average molecular weight.

The initial liquid layer in this investigation is pure water with 8 ppm dissolved O_2. The water layer is included in the model using the same algorithms as in the gas phase. In principle, the water layer is just another region of the plasma—albeit with a higher density and different reaction mechanism. Surface tension is not explicitly calculated in the model—we simply specify the boundary between the liquid and gas phase. However, evaporation of the water layer into the gas phase is included. The methods used to couple the gas phase plasma and the liquid phase calculations, the reaction mechanism, and method for representing water vapor evaporating from the reactive and dielectric water layers (see below) are discussed in [14].

The fluid module is first executed without the plasma to establish the advective flow field. For the geometry and flow rates of interest, the flow field is established in tens of ms of integration time using timesteps that are typically many times the Courant limit for the smallest cells in the mesh. The plasma is then initiated as described below, and the fluid and plasma modules are simultaneously integrated until the voltage pulse is terminated and space charge is allowed to dissipate. At that point, we stop solving Poisson's equation and assume local charge neutrality. The fluid module and continuity equations of individual species continue to be integrated with ns timesteps to account for rapid reactions that initially take place. As the reactivity diminishes, the timesteps grow to 1 μs over 50 ms of flow during which the majority of reactive gaseous species are blown out of the computational domain. At this point, the fluid module is terminated and the reactions of the aqueous species are continued to be solved with a time step of 10–100 μs until the computation is terminated at 10 s.

Based primarily on the dimensions of the KinPen developed by the INP Greifswald [9, 10]. The geometry used in this investigation for the plasma jet is a cylindrical tube with a diameter of 1.6 mm and walls that are 0.4 mm thick. The tip of the coaxial electrode, 0.25 mm in diameter, is 3.5 mm from

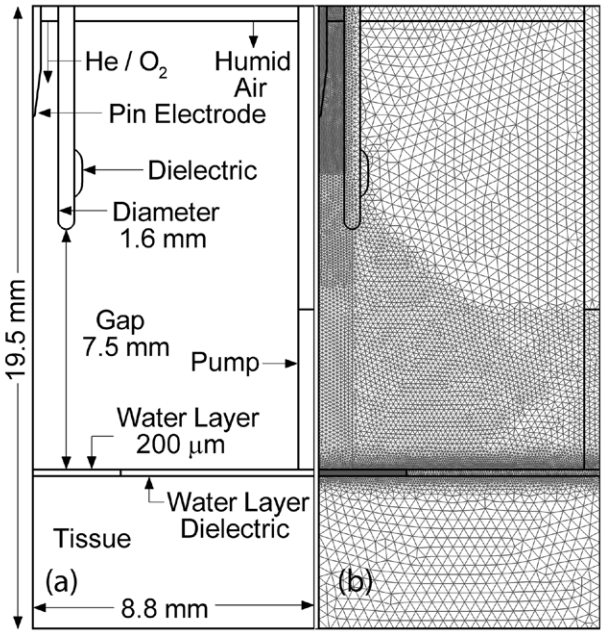

Figure 1. Schematic of the cylindrically symmetric model geometry. (*a*) The total computational domain is 1.95 cm in height and 0.88 cm in radius. (*b*) Numerical mesh showing different refinement zones.

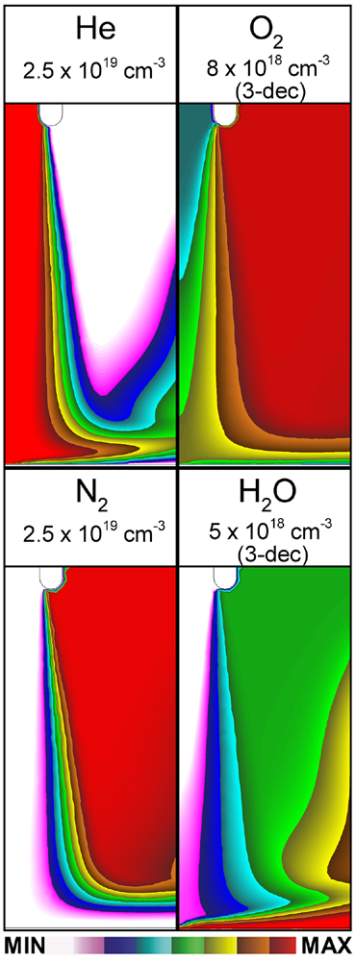

Figure 2. Flow profiles at 8 ms prior to initiating the discharge for (*a*) He, (*b*) O_2, (*c*) N_2 and (*d*) H_2O. The water vapor is blown from the surface of the water layer by the jet. The maximum value is noted in each frame. Contours are on a linear scale unless the number of decades for a log scale is noted.

the end of the tube, as shown in figure 1. In this configuration, there is an axial component of the electric field that better enables the plasma to intersect with the liquid [16, 17]. This configuration differs from those that have an electric field that is dominantly perpendicular to the gas flow and which produces a plume that is dominated by neutral reactive species [18]. The end of the tube is 7.5 mm above a 200 μm thick water layer covering the tissue-like dielectric. The portion of the water treated as plasma extends to a radius of 2.75 mm. For larger radii, the water is not treated as a reactive zone but rather is represented simply as a dielectric material. These separate water zones were implemented to lower the computational cost. Water evaporates from both water zones. The numerical mesh, also shown in figure 1, consists of 12 700 nodes with several refinement zones having spatial resolution varying from 24 μm near the tip of the electrode and within the water layer to 300 μm in the periphery of the domain.

Helium seeded with O_2 (He/O_2 = 99.8/0.2, 5 slm) is flowed through the tube. Humid air ($N_2/O_2/H_2O$ =79.5/20/0.5) flows at a lower rate outside the tube (4 slm) to entrain the helium and guide the helium flow over the surface. The resulting mixture flow out of the computational domain through a pump port on the side boundary. The material for the tube has a dielectric constant $\varepsilon_r = \varepsilon/\varepsilon_o$=4, the tissue underlying the liquid has ε_r = 5 and the non-reactive water layer has ε_r = 80. At the beginning of the plasma period, the voltage pulse is applied for 50 ns (5 ns rise time).

A single discharge pulse of a plasma jet, its afterglow and activation of a thin water layer are discussed here. Actual systems are operated with a pulse-repetition frequency (PRF). Plasma jet treatment of tissue differs significantly from dielectric barrier discharge (DBD) treatment in many ways—one being that the gas in a plasma jet has a finite residence time in the vicinity of the tissue. Depending on flow rates, jet diameter and situational factors (e.g., turbulence, eddies produced by local structures [19]), the gas and plasma may smoothly blow out of the vicinity of the tissue in a laminar manner with air diffusing into the jet or there may be significant recirculation. All of these effects are important to the final fluence of reactants to the tissue underlying the liquid. The results of this study are therefore applicable to conditions of laminar flow with a PRF of less than a few kHz where the plasma activated gas flows out of the volume between pulses.

3. Touching and not-touching plasma jets onto a liquid layer

3.1. Transport of gas phase RONS

The pre-pulse steady-state densities of He, O_2, N_2 and H_2O in the fluid flow-field are shown in figure 2 from the exit nozzle of the jet. Helium flows down from the tube into the ambient air where the helium is largely confined to the center of the

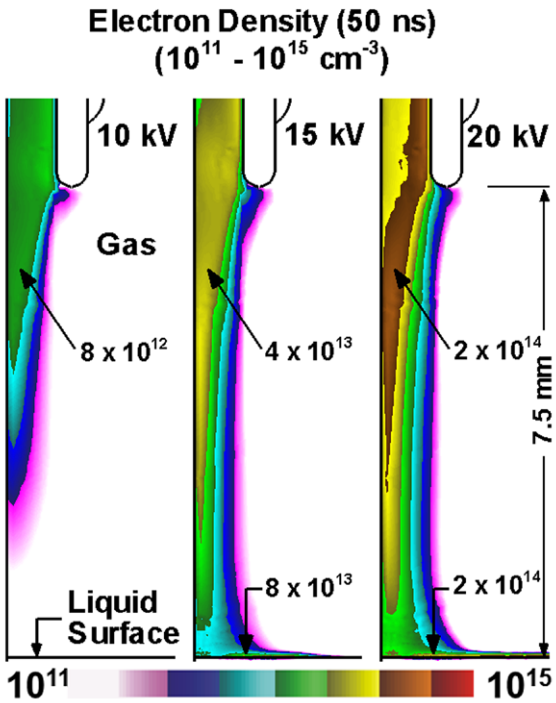

Figure 3. Electron density for applied potentials of −10 kV, −15 kV and −20 kV at 50 ns prior to pulse termination. The electron plume for −10 kV does not touch the liquid surface. The electron plume for −15 kV touches at 35 ns (in contact with water and spreading for 15 ns) and the plume for −20 kV touches at 20 ns (in contact for 30 ns). Contours are on a log-scale over 4 decades.

jet by air diffusing into the core. The He then flows radially outward from the stagnation point on axis. The axial speed of the flow field inside the tube is 42 m s^{-1}. The corresponding Reynolds number is Re = 630, which is less than the value for onset of turbulence for pipe flow, Re = 2 300. So the flow should be laminar leaving the tube. Once the jet leaves the tube, for Re = 630 the onset of turbulence will occur at about $50r_0$ from the outlet, where r_0 is the jet radius [20]. For our conditions, the onset of turbulence would be expected at about 4 cm from the tube outlet, which is larger than our outlet-surface distance. The increase in the He concentration at the right of the panel is a vortex at larger radii. The density of O_2 is shown over three decades to highlight the small amount, 5.9×10^{16}cm^{-3}, contained in the input He gas flow. The diffusion of air into the He jet increases the O_2 concentration to 3.9×10^{17}cm^{-3}, on axis 1 mm above the water. N_2 from the ambient is absent from the interior of the tube and becomes entrained in the He jet further from the exit as air diffuses into the jet stream. The density of N_2 is 1.3×10^{18}cm^{-3} on axis 1 mm above the water. The water vapor that evaporates from the water layer is displaced by the helium jet and flows to the pump. The density of H_2O in the ambient air is 1.2×10^{17}cm^{-3}. Directly above the liquid water on the axis, the density of H_2O is low, $\approx 10^{16}$cm^{-3}, due to the inability for the ambient water vapor to diffuse into the core of the helium jet. The flow of the jet displaces the evaporating water vapor directly above the liquid layer at small radii and compresses the water vapor at larger radii. The reactive species delivered to the surface of the liquid are determined by the species initially produced by electron impact excitation, dissociation and ionization in the plasma plume, their subsequent reactions, convection in the fluid flow field and density gradient driven diffusion.

Plasma jets for three voltages were investigated— − 10 kV, −15 kV and −20 kV. The voltage pulses have a 5 ns rise time and 45 ns duration. A cloud of plasma with density of 10^{11}cm^{-3} and radius 0.7 mm is seeded at the tip of the powered electrode for ignition. The electron densities, n_e, at the end of the discharge pulse for each voltage are shown in figure 3. The electron avalanche begins as an ionization wave at the tip of the pin electrode, and quickly assumes an annular, wall hugging mode [21, 22], which charges the inside surface of the glass tube. As the ionization wave exits the tube, the avalanche returns to the axis. This is the same behavior for all voltages—n_e is annular and surface-hugging inside the tube and transitions to on-axis within a few mm of exiting the tube. The n_e on axis 1 mm from the end of the tube is 6.7×10^{12}cm^{-3}, 2.7×10^{13}cm^{-3}, and 6.9×10^{13}cm^{-3} for −10 kV, −15 kV and −20 kV. In the −10 kV case, the plasma plume, represented by the electron density, does not reach the surface of the water with a significant density and this is considered the indirect, or not-touching, case. The plasma plumes for the −15 kV and −20 kV cases both reach the water and are the direct, or touching cases. The electron density 1 mm above the water layer on axis is 4.2×10^{12}cm^{-3} and 6.7×10^{12}cm^{-3} for the −15 kV and −20 kV cases.

The electron density, electron temperature (T_e) and electron impact ionization source (S_e) are shown in figure 4 for the −15 kV case. The speed of the ionization wave depends on the applied voltage. For the −15 kV case, the electron plume touches the surface of the water at 26 ns. A conducting channel of increasing electron density is produced on axis as the capacitance of the water layer is charged until the voltage is terminated. T_e, and S_e trace the trajectory of the head of the ionization wave (the *plasma bullet*) or guided streamer [8]. T_e and S_e in the head of the plasma bullet midway through the gap are 5 eV and 1×10^{21}cm^{-3} s^{-1}. The mushroom shaped luminous plasma bullet from the simulation before striking the surface of the water layer is similar to those shapes experimentally observed for plasma bullets [23]. Upon striking the water layer, a restrike, positive ionization wave propagates back up the plasma column.

The ionization wave generated in the plasma tube propagates through the helium dominated channel and, if sufficient duration or length, intersects with the liquid layer. Since the liquid layer has largely dielectric properties, the discharge at this point behaves similarly to a DBD—the plasma spreads on the surface of the liquid as the surface charges. This spreading results from many causes. The large dielectric constant of the liquid excludes electric fields, on a relative basis, out of the liquid in favor of the air. The lower electric field and higher neutral density in the water produces a low E/N [electric field/(gas or liquid number density)] that will not self-sustain the plasma. For example, at the instant the ionization wave reaches the surface of the water at 26 ns, the E/N = 60 Td (1 Td = 10^{-17}V cm^2) 25 μm above the surface of the water

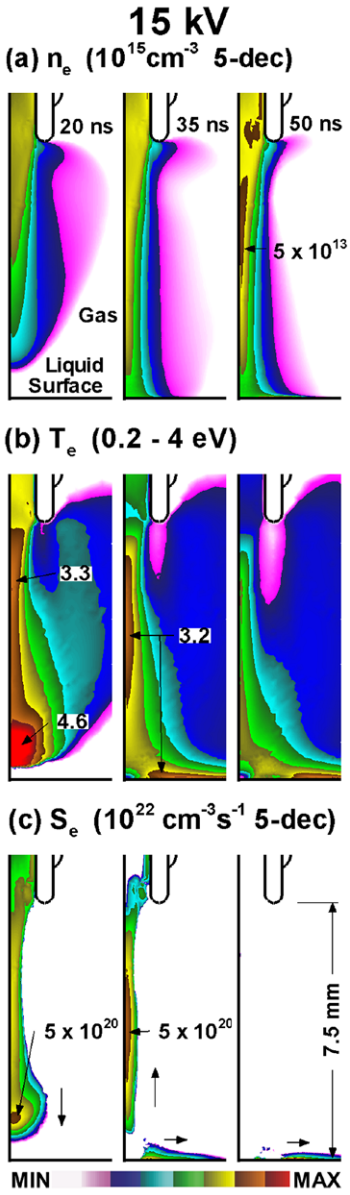

Figure 4. Plasma dynamics −15 kV. (*a*) Electron density, (*b*) electron temperature and (*c*) electron impact ionization source at 20 ns, 35 ns and 50 ns after start of the pulse. At 20 ns the ionization wave has not touched the surface. The spread of the ionization as a surface ionization wave continues after touching. Contours are on a linear scale unless the number of decades for a log scale is noted.

while the E/N = 0.0025 Td 25 μm below the surface of the water. These latter values of E/N are well below that required to self-sustain a plasma. The charged particle inventory in the water is therefore a result of electrons and ions solvating into the liquid, photoionization and water chemistry, and not direct electron impact dissociation and ionization.

There is also *de facto* charging of the surface layer of the liquid due to the long dielectric relaxation time of the low-conductivity water. The solvation of electrons into the water, and charge exchange from positive ions with water molecules, occurs on a ps to ns timescale, transferring charge to the water. The low mobility of these charged species in the water confines the transferred charge to the surface of the water for the duration of the discharge. The charge injection into the water is augmented by photoionization of the water by UV/VUV photons produced by the plasma adjacent to the water. For these conditions, the charge at the surface of the water at the end of the discharge pulse is due 90% from solvation of gas phase charged particles into the liquid and 10% from photoionization.

Plasma plumes that do not touch the water layer lack the nearly immediate electron solvation, charge exchange and photoionization (and photolysis) reactions at the surface of the liquid that result from plasma contact. The spreading of the plasma on the surface of the water is important to the production of charged aqueous species. The solvation of charged species is distributed over a larger radius, and the close contact enables UV/VUV radiation, that has a short mean-free-path, about 12 μm, to penetrate into the water. The electron density in the not-touching plasma plume largely decays due to recombination with molecular ions, dominantly N_4^+ and O_2^+, and electron attachment to O_2 in many to tens of microseconds. This time is short compared to the time for the convective gas flow to reach the liquid, about 0.34 ms. So the vast majority of electrons will have recombined or attached prior to reaching the liquid. The end result is that the effluent of the plume consists of a low density ion-ion plasma. Since the time scale for ion-ion recombination can be commensurate with the time for the convective gas flow to reach the liquid, a low density of ions does reach the water even in the not-touching case. For example, for the −10 kV not-touching case, the maximum gas phase negative ion density adjacent to the water is 10^{10} cm^{-3} at tens of μs after the discharge pulse. Note that this long time scale ion-ion plume occurs for the higher voltages as well. As discussed below, its influence is simply smaller in the touching cases.

The gas dynamics play an important role in distributing gas phase reactive species to the liquid. For example, the density of O_3 is shown in figure 5 for the –15 kV case. The O atoms that produce O_3 by a 3-body reaction with O_2 are formed dominantly inside the tube by electron impact dissociation of the O_2 additive. Since the density of O_2 is low in the tube, the formation of O_3 is low. The formation of O_3 is dominantly outside the tube where the O_2 in the air diffuses into the plasma plume and reacts with the O atoms formed in the tube. Once formed, O_3 is relatively unreactive in the absence of organic impurities in the air, and so flows with the plume to the surface of the liquid. As the plume spreads along the surface of the water, the O_3 solvates to form the terminal species O_{3aq}. The solvation of O_3 is therefore fairly uniform over a large radius. The majority of O_3 flows out of the computational domain. Here is where the details of the local flow dynamics are important. Vortices, turbulence or stagnation-point flow that are produced by, for example, non-vertical jets or the structure of sample-wells will recirculate species such as O_3 back to the water layer instead of directly flowing out of the region of interest.

O_{3aq} largely results from solvation of gas phase O_3 and the production of O_3 depends largely on the inventory of O atoms produced by the discharge. The formation of O_3 is therefore

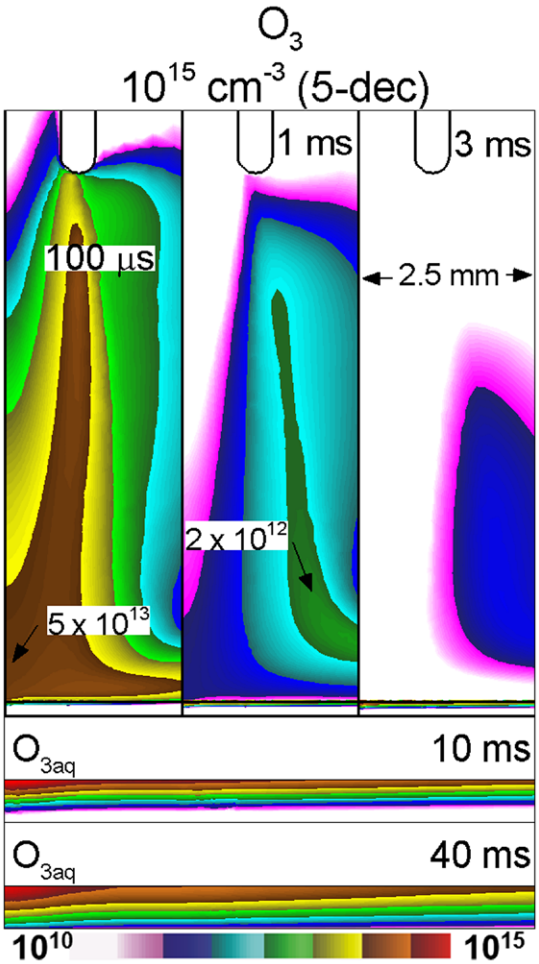

Figure 5. Ozone density in the gas phase and in the liquid for −15 kV at varying times after the discharge pulse. Ozone is relatively non-reactive in both phases. Contours are on a 5-decade log-scale.

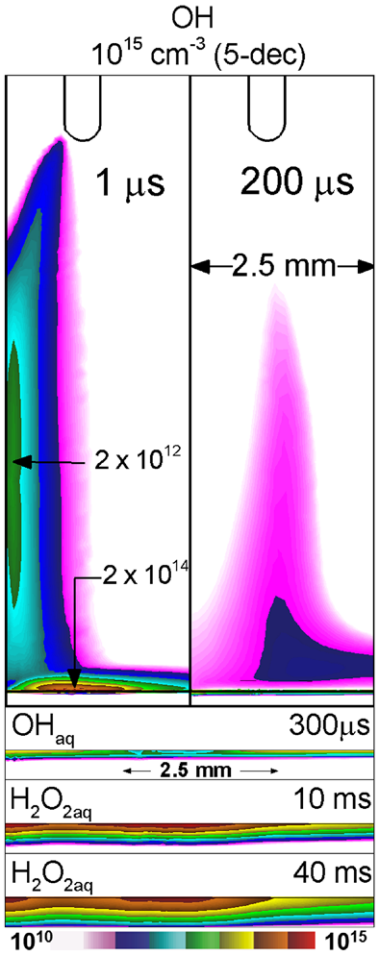

Figure 6. OH in the gas phase and water, and H_2O_2 in the water for the −15 kV case at varying times after the discharge pulse. At 1 μs, the highest OH concentration is adjacent to the water layer where the electron plume intersects the evaporating water. Over the next 200 μs the OH reacts or blows away. The evolution of OH_{aq} into H_2O_{2aq} is shown in the lower panels. Notice that the location of the high concentration of OH at 1 μs becomes the location of the highest concentration of H_2O_{2aq}. Contours are on a 5-decade log-scale.

only weakly dependent on whether the plasma touches or does not tough the liquid, other than plasma touching plumes are typically of longer duration and so produce more O atoms in the vicinity of the liquid. The maximum O_3 density 1 mm above the liquid layer at 100 μs is 1.1×10^{13} cm^{-3}, 4.6×10^{13} cm^{-3}, and 1.4×10^{14} cm^{-3} for −10 kV, −15 kV and −20 kV. The end result is that O_{3aq} is produced in large amounts in both the touching and not-touching cases.

The production of the hydroxyl radical, OH, in the gas phase significantly differs from that of O_3. OH is initially formed by electron impact dissociation of H_2O during the interaction of the plasma and the humidity in the air and, more importantly, the evaporated water vapor above the water layer. The density of OH is shown in figure 6 at 1 μs and 200 μs after the discharge pulse for the −15 kV case. OH is largely produced in the plasma column by electron impact dissociation of water diffusing into the jet, generating a maximum density of 2.2×10^{12} cm^{-3} at mid-gap at the end of the pulse. A larger density is produced adjacent to the water by the spreading plasma over the liquid intersecting with the evaporating water vapor. The maximum OH density adjacent to the water is 7.2×10^{14} cm^{-3} at the end of the discharge pulse. Although the production of OH does not significantly change in mid-gap for the touching and not-touching cases beyond the change in energy deposition (8.0×10^{11} cm^{-3}, 2.2×10^{12} cm^{-3}, and 8.5×10^{12} cm^{-3} for −10 kV, −15 kV and −20 kV), the absence of spreading of the plasma on the liquid in the not-touching case significantly reduces the inventory of OH available. The OH mutually reacts to form H_2O_2, reacts with nitrogen atoms to form NO, solvates into the water to form OH_{aq}, or blows away within a few ms with the flow.

Photolysis of the water also produces OH_{aq}. The production of OH_{aq} by photolysis is less than 1% in the not-touching case and 10% in the touching case. The reason for more photolysis producing OH_{aq} in the touching case is that electron impact excitation produces $N_2(b'\Pi_u)$ in the immediate vicinity of the surface of the water by the surface hugging plasma. VUV photons emitted by $N_2(b'\Pi_u)$ are then able to reach the water prior to being absorbed in the humid air. By mutual reaction of OH_{aq}, H_2O_{2aq} is produced which is also largely a terminal species in the absence of organic matter in the liquid. As shown in figure 6, the high concentrations of OH at 1 μs resulting from

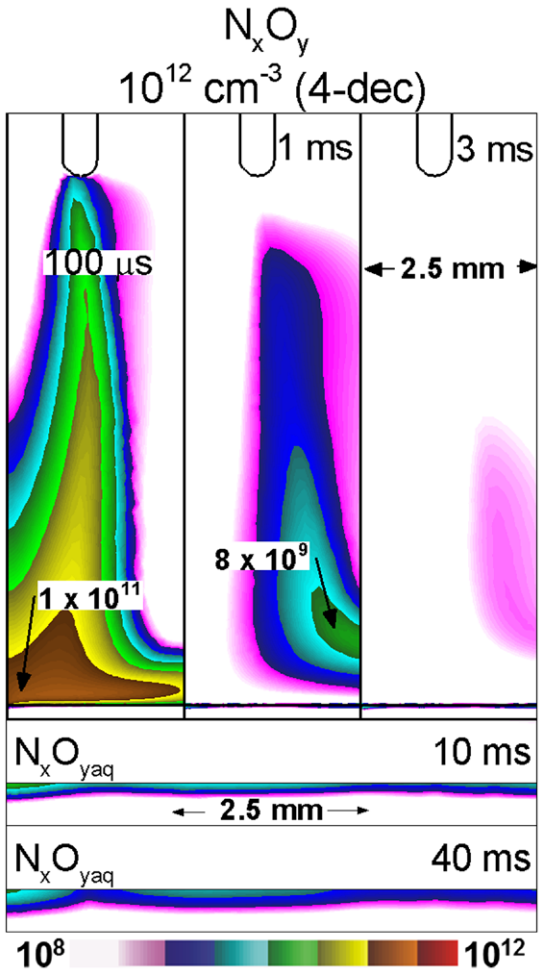

Figure 7. N_xO_y density for the −15 kV case shown at varying times after the discharge pulse in the gas and water layer. NO is the initiating molecule for producing N_xO_y. The comparatively low density of N_xO_y results from the effectiveness of the helium jet blocking access of NO to the water layer and the laminar flow that blows NO away. Contours are on a 4-decade log-scale.

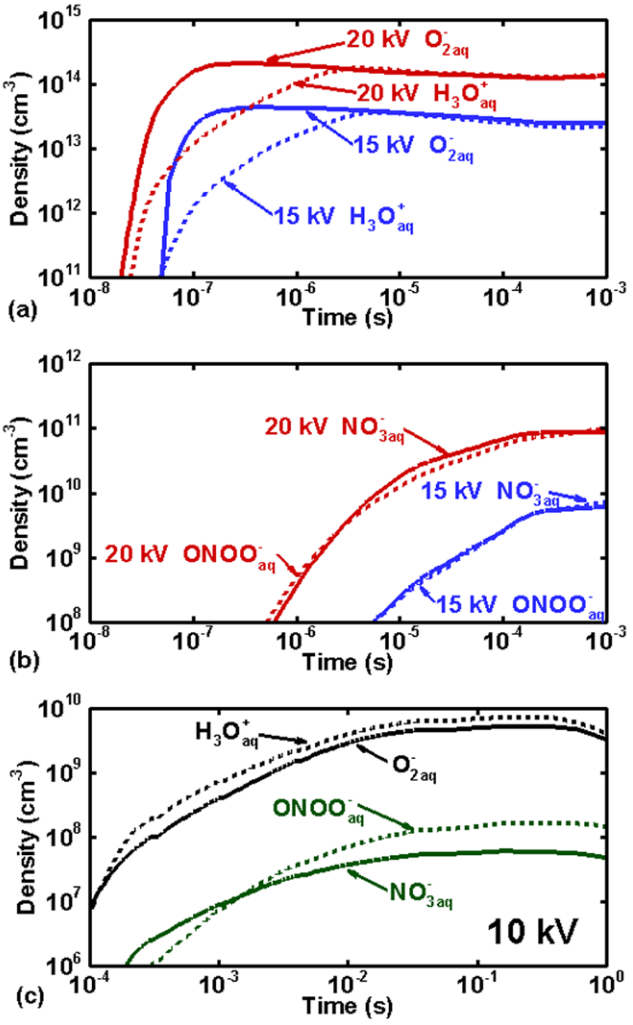

Figure 8. The time evolution of the liquid volume average densities of aqueous ions. (*a*) $O_2^-{}_{aq}$ and $H_3O^+_{aq}$; and (*b*) $NO_3^-{}_{aq}$ and $ONOO^-_{aq}$ for the touching −15 kV and −20 kV cases. (*c*) Densities for the −10 kV (not-touching) case.

spreading of the plasma through the evaporating water vapor produces a distribution of OH_{aq} having a maximum density of 2.2×10^{14} cm^{-3} or (3.7×10^{-7} M) at a radius of 1 mm. The primary loss mechanism for OH_{aq} is the reaction forming H_2O_{2aq}, $OH_{aq} + OH_{aq} \rightarrow H_2O_{2aq}$. The lifetime of OH_{aq} based on this maximum density and rate coefficient of 5.5×10^9 M^{-1} s^{-1} [14, 24] is about 0.25 ms. The resulting H_2O_{2aq} then diffuses through the water layer to the underlying tissue.

Reactive nitrogen species (RNS), N_xO_y, consist of the sum of NO, NO_2, NO_3, N_2O_3, N_2O_4 and N_2O_5. RNS are formed as the plasma plume reacts with the ambient air as shown in figure 7. Nitrogen oxide (NO) is initially formed primarily by reaction of N atoms with O_2. The N atoms are formed dominantly by the electron impact dissociation of N_2 resulting from air diffusing into the plume. Since the He flow from the jet displaces air at the surface of the water and there is no N_2 injected through the tube, the RNS are primarily produced at the edge of the plasma jet where air diffuses into the plume. The precursor species to N_xO_y, NO, is largely formed at the boundary of the plasma where the density of the N_2 is largest and secondarily in the core of the plasma plume where the O atom density is the highest. The N_xO_y that are formed from the plasma discharge reacting with the ambient air react further react with OH and HO_2 in the ambient to form HNO_2, HNO_3 and HOONO. The large densities of N_xO_y produced in, for example, DBDs accumulates over thousands of pulses and can reach 3×10^{17} cm^{-3} in DBDs sustained in non-flowing air [25]. In the absence of vortices or other forms of recirculation in the gas phase, the NO and NO_2 that would normally be the starting point for forming higher N_xO_y in stagnant systems are blown out of the volume in plasma jets. The density of higher N_xO_y and acids HNO_x are therefore small compared to DBDs, reaching a maximum density 1 mm above the liquid of only 2×10^{11} cm^{-3} during the single pulse.

3.2. Evolution of aqueous reactivity

The gas phase species in contact with the water then solvate to form aqueous species. The densities of aqueous ions averaged over the water layer as a function of time are shown in figure 8 for the −10 kV, −15 kV and −20 kV cases. Positive water ions are produced by charge exchange from gas phase

positive ions striking the water and by photoionization. The $H_2O^+_{aq}$ then quickly charge exchange with water to produce hydronium, $H_3O^+_{aq}$ and hydroxyl radicals, OH_{aq}. $H_3O^+_{aq}$ is a terminal species that dominates the positive ions and whose density is largely established by 1 ms after the discharge pulse. The average density of $H_3O^+_{aq}$ in the water layer is 2×10^{14} cm^{-3} and 3×10^{13} cm^{-3} for the −20 kV and −15 kV cases. The aqueous anions are initially formed by solvated electrons dissociatively attaching with H_2O_{aq} to form OH^-_{aq} or by attaching to the dissolved O_{2aq} to form $O_2^-{}_{aq}$. The OH^-_{aq} then combines with $H_3O^+_{aq}$ or OH_{aq} to form OH_{aq} and O^-_{aq} respectively. The O^-_{aq} then combines with O_{2aq} to form the terminal negative ion $O_3^-{}_{aq}$. In the absence of significant densities of N_xO_{yaq}, the long lived $O_2^-{}_{aq}$ and $O_3^-{}_{aq}$ dominate the negative ions.

As shown in figure 8 for −20 kV, $O_2^-{}_{aq}$ is quickly formed during the discharge pulse by attachment of solvated electrons to dissolved O_2 as the plasma touches and spreads on the surface of the water. The time for electron solvation is only tens of ps and the density of solvated electrons reaches its maximum value of 2.1×10^{14} cm^{-3} within 200 ns. The density of $H_3O^+_{aq}$ develops over a few μs since up to two charge exchange reactions are required for its formation—solvating ions reacting with water to form $H_2O^+_{aq}$, and then a second reaction with water to form $H_3O^+_{aq}$. There is also a contribution to $H_3O^+_{aq}$ by hydrolysis of HNO_{xaq}, however since the density of the acids is low, this is a minor contribution. The densities of $O_2^-{}_{aq}$ and $H_3O^+_{aq}$ for −15 kV show the same trends as for −20 kV. The initial rise in densities for −15 kV are delayed in time by about 20 ns compared to −20 kV, which is the difference in arrival times of the electron plumes at the surface of the water. The densities are also decreased by a factor of 5–6, a consequence of the shorter length of time that the surface ionization wave spreads on the water at the lower voltage.

The electron plume does not reach the water layer with a significant density for the −10 kV case and so there is no prompt formation of aqueous ions. As noted above, the electron-ion plume transitions to an ion-ion plume as recombination and attachment reduce the electron density. This recombining ion-ion plume then intersects with the water layer on up to a ms timescale, which is the time required for the plume containing the ion-ion plasma to cross the gap. Upon intersection with the water, the low density of gas phase ions (10^{10} cm^{-3} at 10 μs) solvate into the water over several ms, producing average aqueous densities of $>10^9$ cm^{-3}. $O_2^-{}_{aq}$ and $H_3O^+_{aq}$ are produced in a similar manner as described above for the higher voltages, evolving over 10s to 100s ms to produce an aqueous density of nearly 10^{10} cm^{-3}, a factor of 10^4 smaller than for the touching cases. This same, longer time solvation of the ion-ion plume also occurs for the higher voltages. However, the contribution of the ion-ion plasma plume to aqueous ion formation is simply smaller than the direct solvation of the electron-ion plasma in contact with the water.

The N_xO_y that reaches the water also solvates into the liquid, where N_xO_{yaq} eventually forms HNO_{2aq}, HNO_{3aq} and $HOONO_{aq}$ [14]. HNO_{2aq} is a weak acid so only about 1% of its concentration hydrolyzes to $H_3O^+_{aq}$ and $NO_2^-{}_{aq}$. HNO_{3aq} and $HOONO_{aq}$ are strong acids and nearly completely hydrolyze to form $H_3O^+_{aq}$, $NO_3^-{}_{aq}$ and $ONOO^-_{aq}$. The terminal anions for N_xO_{yaq} species are $NO_3^-{}_{aq}$ and $ONOO^-_{aq}$. Since the majority of N_xO_y that solvates in the water is not formed in the spreading plasma on the surface, these molecules must convect and diffuse from more remote locations. This convection requires about 1 ms for the touching cases, resulting in the $NO_3^-{}_{aq}$ and $ONOO^-_{aq}$ reaching a maximum density of 10^{11} cm^{-3} for −20 kV and 10^{10} cm^{-3} for −15 kV. The same process requires tens of ms in the not-touching cases producing a density of 10^8 cm^{-3}. The dynamics of N_xO_y for DBDs in stagnant gases and in jets do significantly differ. In stagnant DBDs, N_xO_y accumulates in the gas phase, diffuses into the water and hydrolyzes. In jets, there are shorter residence times for the N_xO_y in the gas phase due to the convective flow and so less opportunity to accumulate to large densities. The result is less hydrolysis in the water and low densities of nitrates and nitrites in the liquid. For both types of plasmas sources, N_xO_{yaq} will accumulate in the liquid phase over successive discharge pulses.

The densities of neutral aqueous species averaged over the water layer as a function of time are shown in figure 9 for the −10 kV, −15 kV and −20 kV cases. In the touching cases (−15 kV, −20 kV), the OH_{aq} has a rapid rise during the discharge pulse (tens of ns) due to photolysis, augmented on the hundreds ns time scale by charge exchange reactions forming $H_3O^+_{aq}$ and OH_{aq}. The maximum densities for OH_{aq} are 5.8×10^{14} cm^{-3} for −20 kV and 7.4×10^{13} cm^{-3} for −15 kV. The majority of OH_{aq} is expended in forming H_2O_{2aq}, whose maximum densities of 2.7×10^{14} cm^{-3} for −20 kV and 4.4×10^{13} cm^{-3} for −15 kV are reached in about 1 ms. The H_{aq} that is produced by photolysis of H_2O_{aq} reacts with the dissolved O_{2aq} to form HO_{2aq}, which is also formed by O_{aq} reacting with OH_{aq}. As the OH_{aq} converts to H_2O_{2aq} over time in the water layer, the primary loss mechanisms for HO_{2aq} become reactions with NO_{aq} to form HNO_{3aq} or hydrolysis to form $H_3O^+_{aq}$ and $O_2^-{}_{aq}$. The density of HO_{2aq} rises during the discharge pulse due primarily to the source of H_{aq} in photolysis reactions (6×10^{14} cm^{-3} for −20 kV and 7×10^{13} cm^{-3} for −15 kV) and slowly declines on ms timescales as NO solvates to form NO_{aq}. Since the source of O_{3aq} is dominated by diffusion of O_3 from the gas phase, its density increases over many ms with maximum values of 2.1×10^{14} cm^{-3} for −20 kV and 5.6×10^{13} cm^{-3} for −15 kV.

The time evolution of OH_{aq} for the not-touching case (−10 kV) significantly differs from the touching cases. Lacking the photolysis and charge exchange reactions which produce OH_{aq} on ns timescales as for touching cases, diffusion of OH into the water and dissociative excitation transfer to water molecules by $N_2(A)$ produce OH_{aq} over hundreds of μs. Note that the rise of O_{3aq} shadows that of OH_{aq} as both require diffusion of neutral species from the gas phase for their formation in the liquid. The maximum densities of O_{3aq} and OH_{aq} are 6.4×10^{12} cm^{-3} and 2.8×10^{12} cm^{-3}. The OH_{aq} converts to H_2O_{2aq} whereas O_{3aq} is a terminal species. The density of OH_{aq} falls below that of H_2O_{2aq} within 1 μs, in agreement with Tresp *et al* [7]. The formation of the other major neutral aqueous species is less dependent on the plasma striking the surface than for ion species. An exception is HO_{2aq} whose formation benefits from the production of H_{aq}

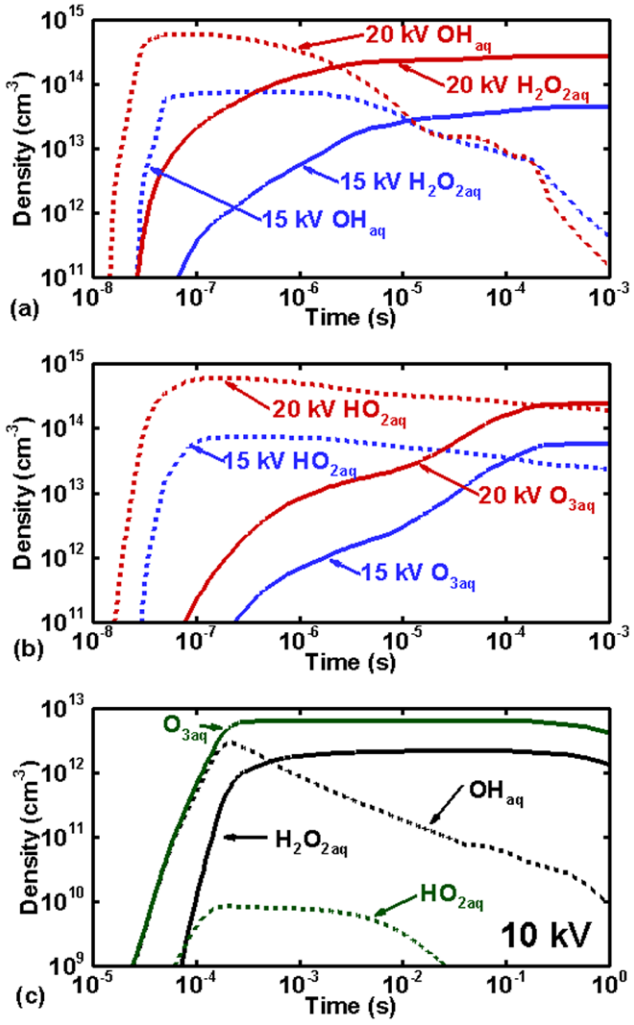

Figure 9. The time evolution of the liquid volume average densities of neutral aqueous species (*a*) H_2O_2aq and OH_{aq}; and (*b*) O_3aq and HO_{2aq} for the touching −15 kV and −20 kV cases. (*c*) Densities for the −10 kV (not-touching) case.

during photolysis reactions which have at best a minor role in the not-touching case. As a result, HO_{2aq} is disproportionately smaller for the −10 kV case.

3.3. Fluences to the tissue

The treatment of the underlying tissue ultimately depends on the fluence of reactive species that transport through the liquid layer. These fluences are shown in figure 10 after 10 s following a single discharge pulse. The maximum fluences for $H_3O^+_{aq}$ and $O_2^-{}_{aq}$ for −20 kV are 3×10^{11} cm^{-2}. For the −15 kV touching case, the fluences are reduced by a factor of 10. This reduction is largely a consequence of the shorter time the plasma spreads on the liquid for −15 kV. The production of aqueous ions by the ion-ion plume for −10 kV is smaller by a factor of 10^4. The low rate of solvation of N_xO_y to form aqueous RNS is reflected in the small fluences of $NO_3^-{}_{aq}$ and $ONOO^-{}_{aq}$ to the tissue, and which is only significant in the high voltage case. The neutral species are less affected by the touching or not-touching conditions. For example, the formation of O_{3aq}

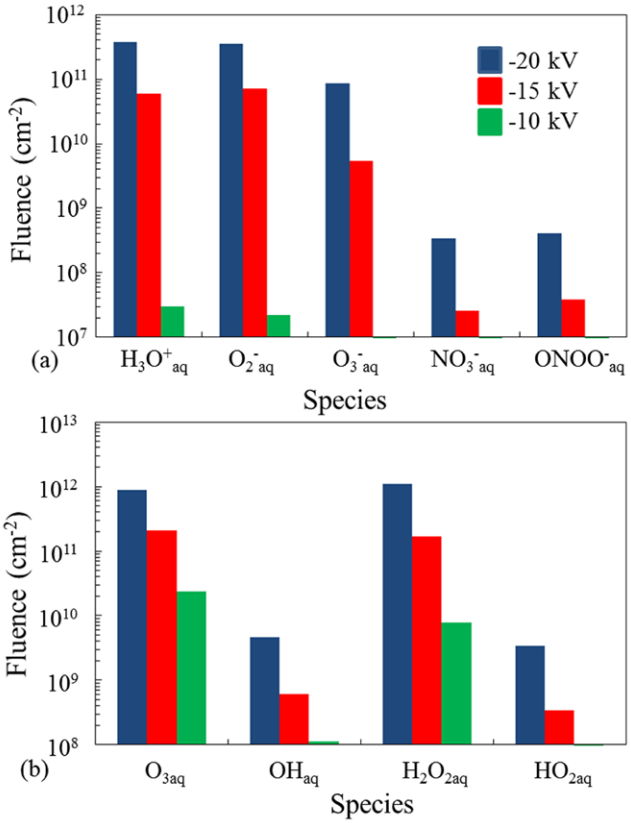

Figure 10. Fluences to the tissue beneath the water over 10 s for not-touching (−10 kV) and touching (−15 kV, −20 kV) cases. (*a*) Ions and (*b*) neutral species.

results from the advective flux of O_3 from above the water layer, a process which is not particularly sensitive to touching or not-touching conditions. So the fluence of O_{3aq} is largely a function of energy deposition and decreases in proportion to the applied voltage (4 times more energy per pulse for −20 kV compared to −10 kV). The fluence of H_2O_{2aq} to the tissue has a larger decrease with decreasing voltage than O_{3aq} due to the contribution of photolysis and charge exchange to formation of its precursor OH_{aq}. However this decrease in H_2O_{2aq} is small compared to the ions—a consequence of a large fraction of OH_{aq} originating from diffusion of neutral species into the water. The fluence of HO_{2aq} for the not-touching case is not appreciable, as its formation depends on the production of H atoms by photolysis which is only significant for touching cases.

3.4. Electric fields

Another factor which is sensitive to the plasma jet touching or not-touching the liquid is the delivery of electric fields to the tissue underlying the liquid. The maximum electric field at the surface of the tissue occurs at the end of the discharge pulse for the −10 kV, not-touching, case and is 1 kV cm^{-1}. For the touching cases, the maximum electric field at the surface of the tissue occurs within 5–10 ns of the ionization wave striking the water layer and reaches a value of 14 kV cm^{-1} for the −15 kV case and 17 kV cm^{-1} for the −20 kV case. From

shortly after impact of the ionization wave until the pulse terminates, the magnitude of the electric field decreases by only a few $kV\,cm^{-1}$. Once the voltage is removed, the field quickly dissipates as the charge density on the surface of the water decreases. These values of electric field for a single pulse, up to $20\,kV\,cm^{-1}$ for tens of ns, are near the threshold for producing electroporation [26]. The threshold electric field for electroporation decreases with increasing number of pulses, and so the potential for producing electroporation with touching plumes may be significant at high PRF.

4. Concluding remarks

One of the major distinctions in producing active aqueous species in water layers over tissues by plasma jets is whether the visible electron-ion plasma plume touches the surface of the water. There are at least two major modes for delivery of active species to the water layer. The first can dominate in touching cases—the spreading of plasma over the liquid surface. This immediate proximity of the plasma to the liquid enables photolysis, direct charge exchange reactions with H_2O_{aq}, and direct solvation of electrons. The longer the dwell time of the plasma on the surface of the liquid, the more aqueous ions and photolysis products are formed over a larger area. Species such as HO_{2aq} that trace their origins to these reactions are also produced in larger numbers. Not-touching plasmas do receive fluxes of gas phase ions in the form of an ion-ion plume, however these fluxes can be orders of magnitude smaller than in the touching cases.

The second mode of delivery is convection and diffusion of neutral species to the liquid which are formed remotely from the surface. The formation of aqueous reactivity by neutral species is much less sensitive to touching or not-touching conditions, as demonstrated by the commensurate, voltage scaled fluences of O_{3aq} to the tissue discussed here. The delivery of these neutral species to the water is more sensitive to fluid dynamics than for the ions. Vortices, turbulence and other forms of recirculation that extend the residence time of neutral species at the surface of the water increases the likelihood of their solvation. This is particularly the case for N_xO_y species that typically accumulate over many discharge pulses in DBDs sustained in non-flowing gas. For strictly laminar, non-vortexed flows, N_xO_y must diffuse through the He core of the jet to reach the surface, and is more likely to be blown away before solvating in significant amounts.

Acknowledgements

This work was supported by the Department of Energy Office of Fusion Energy Science (DE-SC0001319) and the National Science Foundation (CHE-1124724).

References

[1] Laroussi M, Kong M, Morfill G and Stolz W 2012 *Plasma Medicine: Applications of Low-Temperature Gas Plasmas in Medicine and Biology* (Cambridge: Cambridge University) pp 239–60

[2] Kong M G, Kroesen G, Morfill G, Nosenko T, Shimizu T, van Dijk J and Zimmerman J L 2009 Plasma medicine: an introductory review *New J. Phys.* **11** 115012

[3] Laroussi M 2009 Low-temperature plasmas for medicine? *Trans. Plasma Sci.* **37** 714

[4] Rhoades R A and Bell D R 2012 *Medical Physiology: Principles for Clinical Medicine* 4th edn (Baltimore: Williams & Wilkins) pp. 167–77

[5] van Gils C A J, Hofmann S, Boekema B K H L, Brandenburg R and Bruggeman P J 2013 Mechanisms of bacterial inactivation in the liquid phase induced by a remote RF cold atmospheric pressure plasma jet *J. Phys. D: Appl. Phys.* **46** 175203

[6] Lukes P, Dolezalova E, Sisrova I and Clupek M 2014Aqueous-phase chemistry and bactericidal effects from an air discharge plasma in contact with water: evidence for the formation of peroxynitrite through a pseudo-second-order post-discharge reaction of H_2O_2 and HNO_2 *Plasma Sources Sci. Technol.* **23** 015019

[7] Tresp H, Hammer M U, Winter J, Weltmann K-D and Reuter S 2013 Quantitative detection of plasma-generated radicals in liquids by electron paramagnetic resonance spectroscopy *J. Phys. D: Appl. Phys.* **46** 435401

[8] Lu X, Naidis G V, Laroussi M and Ostrikov K 2014 Guided ionization waves: theory and experiments *Phys. Rep.* **540** 123

[9] Reuter S, Tresp H, Wende K, Hammer M, Winter J, Masur K, Schmidt-Bleker A and Weltmann K-D 2012 From RONS to ROS: tailoring plasma jet treatment of skin cells *Trans. Plasma Sci.* **40** 2986

[10] Reuter S, Winter J, Schmidt-Bleker A, Tresp H, Hammer M and Weltmann K-D 2012 Controlling the ambient air affected reactive species composition in the effluent of an argon plasma jet *Trans. Plasma Sci.* **40** 2788

[11] Bruggeman P 2014 private communication

[12] Lay B, Moss R, Rauf S and Kushner M 2003 Breakdown processes in metal halide lamps *Plasma Sources Sci. Technol.* **12** 8

[13] Xiong Z and Kushner M J 2010 Surface corona-bar discharges for production of pre-ionizing UV light for pulsed high-pressure plasmas *J. Phys. D: Appl. Phys.* **43** 505204

[14] Tian W and Kushner M J 2014 Atmospheric pressure dielectric barrier discharges interacting with liquid *J. Phys. D: Appl. Phys.* **47** 165201

[15] Bhoj A N and Kushner M J 2007 Continuous processing of polymers in repetitively pulsed atmospheric pressure discharges with moving surfaces and gas flow *J. Phys.* D **40** 6953

[16] Walsh J and Kong M 2008 Contrasting characteristics of linear-field and cross-field atmospheric plasma jets *Appl. Phys. Lett.* **93** 111501

[17] Lu X, Ziang J, Xiong Q, Targ Z, Hu X and Pan Y 2008 An 11cm long atmospheric pressure cold plasma plume for applications is plasma medicine *Appl. Phys. Lett.* **92** 081502

[18] Maletic D, Puac N, Lazovic S, Malovic G, Gans T, Schulz-von der Gathen V andLj Petovic Z 2012 Detection of atomic oxygen and nitrogen created in a radio-frequency-driven micro-scale atmospheric pressure plasma jet using mass spectroscopy *Plasma Phys. Control. Fusion* **54** 124046

[19] Robert E, Sarron V, Darny T, Ries D, Dozias S, Fontane J, Joly L and Pouvesle J-M 2014 Rare gas flow structuration in plasma jet experiments *Plasma Sources Sci. Technol.* **23** 012003

[20] Bogey C and Bailly C 2010 Direct and large-eddy simulation VII *Proceedings of the Seventh International ERCOFTAC Workshop on Direct and Large Scale Eddy Simulation VII (Trieste, Italy)* ed V Armenio *et al* (Berlin: Springer)

[21] Karakas E, Akman M A and Laroussi M 2012 The evolution of atmospheric-pressure low-temperature plasma jets: jet current measurements *Plasma Sources Sci. Technol*. **21** 034016

[22] Jiang N, Ji A and Cao Z 2010 Atmospheric pressure plasma jets beyond ground electrode as charge overflow in a dielectric barrier discharge setup *J. Appl. Phys*. **108** 033302

[23] Hubner S, Hofmann S, van Veldhuizen E M and Bruggeman P J 2013 Electron densities and energies of a guided argon streamer in argon and air environments *Plasma Sources Sci. Technol*. **22** 065011

[24] Madden K P and Mezyk S P 2011 A critical review of aqueous solution reaction rate constants for hydrogen atoms *J. Phys. Chem. Ref. Data* **40** 023103

[25] Sakiyama Y, Graves D, Change H-W, Shimizu T and Morfill G E 2012 Plasma Chemistry model of surface micro-discharge in humid air and dynamics of reactive neutral species *J. Phys.* D **45** 425201

[26] Beebe S J, Blackmore P F, White J, Joshi R P and Schoenbach K H 2004 Nanosecond pulsed electric fields modulate cell function through intracellular signal transduction mechanisms *Physiol. Meas.* **25** 1077